Hollow Mesoporous Aluminosilica Spheres with Perpendicular Pore Channels as Catalytic Nanoreactors

Xiaoliang Fang,[†] Zhaohui Liu,[†] Ming-Feng Hsieh,[‡] Mei Chen,[†] Pengxin Liu,[†] Cheng Chen,[†] and Nanfeng Zheng[†,*]

[†]State Key Laboratory for Physical Chemistry of Solid Surfaces and Department of Chemistry, College of Chemistry and Chemical Engineering, Xiamen University, Xiamen 361005, China and [‡]Department of Chemical Engineering, University of California, Santa Barbara, California 93106, United States

ABSTRACT The design and synthesis of hollow/yolk-shell mesoporous structures with catalytically active ordered mesoporous shells can infuse new vitality into the applications of these attractive structures. In this study, we report that hollow/yolk-shell structures with catalytically active ordered mesoporous aluminosilica shells can be easily prepared by using silica spheres as the silica precursors. By simply treating with a hot alkaline solution in the presence of sodium aluminate ($NaAlO_2$) and cetyltrimethylammonium bromide (CTAB), solid silica spheres can be directly converted into high-quality hollow mesoporous aluminosilica spheres with perpendicular pore channels. On the basis of the proposed formation mechanism of etching followed by co-assembly, the synthesis strategy developed in this work can be extended as a general strategy to prepare ordered mesoporous yolk-shell structures with diverse compositions and morphologies simply by replacing solid silica spheres with silica-coated nanocomposites. The reduction of 4-nitrophenol with yolk-shell structured Au@ordered mesoporous aluminosilica as the catalyst has clearly demonstrated that the highly permeable perpendicular pore channels of mesoporous aluminosilica can effectively prevent the catalytically active yolk from aggregating. Furthermore, with accessible acidity, the yolk-shell structured ordered mesoporous aluminosilica spheres containing Pd yolk exhibit high catalytic activity and recyclability in a one-pot two-step synthesis involving an acid catalysis and subsequent catalytic hydrogenation for desired benzimidazole derivative, which makes the proposed hollow ordered aluminosilica spheres a versatile and practicable scaffold for advanced catalytic nanoreactor systems.

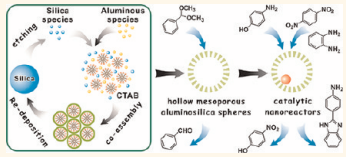

KEYWORDS: hollow structure · ordered mesoporous aluminosilica · perpendicular pore channels · yolk-shell structure · nanoreactor · multiple catalyst

Hollow mesoporous structures have emerged as rapidly growing research themes and have been widely applied in many important research fields,[1−8] such as catalysis,[3] controlled release,[4] confined synthesis,[5] optics and electronics,[6,7] and energy storage,[8] owing to their properties of low density, high surface areas, and interstitial hollow spaces. As a special class of hollow mesoporous structures, the interior of hollow mesoporous structures decorated by encapsulating guest species, which are called "yolk-shell" or "rattle" structures, has attracted tremendous interest in recent years.[9−25] With permeable shells and the unique structures of functional cores, yolk-shell mesoporous structures can provide opportunities to render and advance the applications of hollow mesoporous materials.[9−25] Significantly, since each functional core in the yolk-shell mesoporous structure is isolated by a permeable shell and has a relatively homogeneous surrounding environment, sintering between functional cores can be effectively hindered even under harsh conditions. Hollow mesoporous structures incorporated with catalytically active cores (*i.e.*, sintering-resistant yolk-shell mesoporous structures) have therefore presented promising applications as nanoreactors for catalysis.[11−16]

In the past decade, efforts have been made in the design and synthesis of hollow/yolk-shell mesoporous structures with desired components.[9−24] Several synthetic strategies for hollow/yolk-shell mesoporous structures have been developed, including well-known hard/soft-templating methods,[11−21,26,27] Kirkendall[28] or Ostwald ripening effect,[29] ship-in-bottle techniques,[30] and selective etching.[31−34] Among these strategies, hard-templating is an effective method through which the shape and cavity sizes of hollow/yolk-shell mesoporous structures can be easily and precisely controlled by preprepared templates.[35] Silica nanospheres, including core−shell structure, have been widely used as hard templates.[11−16] The success in the synthesis of hollow/yolk-shell mesoporous structures with various shell components and functional cores makes silica-based templating methods general and effective routes to synthesize hollow/yolk-shell mesoporous structures. However, like other synthetic strategies, silica-based

* Address correspondence to nfzheng@xmu.edu.cn.

Received for review March 16, 2012 and accepted April 13, 2012

Published online April 13, 2012
10.1021/nn3011703

templating methods were ineffective for controlling pore structures, resulting in hollow/yolk-shell mesoporous structures with disordered pore arrangements.[9−24] Ordered mesoporous structures are attractive because their large surface areas, high porosities, and uniform adjustable pore dimensions have been shown to have desired properties in catalysis and biomedical applications.[36−38] Until now, there are, however, only a few examples of hollow/yolk-shell mesoporous materials with ordered mesoporous silica shells which were synthesized using vesicles[26] or polystyrene spheres[39] as templates. It remains a great challenge to develop simple and effective synthesis strategies for preparing hollow/yolk-shell mesoporous materials with ordered pore structures using silica-based templates.

Moreover, although yolk-shell materials with various compositions have been prepared, most studies focus on syntheses of desired catalytically active cores, and rare work succeeds in designing and utilizing catalytically active mesoporous shells.[11−16] Since the core is the sole catalytic component and the permeable shell is only responsible for preventing aggregation from cores, yolk-shell nanoreactors previously reported were usually applied in single-step reactions.[11−16] In modern synthetic chemistry, syntheses of complex molecules are in general multistep reactions. If multistep reactions could be carried out using a multifunctional catalyst to give desired products in high yields, it can significantly reduce the number of purification and separation steps, the amount of wastes and solvents, and thus the cost of final products.[40] The design and synthesis of a multifunctional nanoreactor system employing yolk-shell mesoporous structures with catalytically active ordered mesoporous shells would open new opportunities for their applications in one-pot multistep catalysis.

Herein, we report a facile, effective, and scalable route to prepare catalytically active hollow mesoporous aluminosilica spheres (designated as HMAS) with ordered pore arrangements. Simply by alkaline etching of solid silica spheres in the presence of cationic surfactant and aluminate species, size-controllable HMAS with perpendicular pore channels can be easily obtained. Since silica spheres are used as the template, the synthetic strategy developed in this work can be extended as an effective route to produce yolk-shell mesoporous structures with diverse compositions and morphologies. To the best of our knowledge, it is the first time that yolk-shell mesoporous structures are prepared with catalytically active ordered mesoporous aluminosilica shells. The as-synthesized hollow and yolk-shell mesoporous aluminosilica spheres were applied in heterogeneous acidic catalysis and confined catalysis, respectively. On the basis of available acid activity, the yolk-shell structures reported here can be used as multiple catalysts for multistep reactions in one-pot reactions. From the viewpoint of fundamental research and practical application, such a yolk-shell catalyst system provides a powerful platform for designing novel nanoreactors for catalysis.

RESULTS AND DISCUSSION

Synthesis and Characterization of HMAS. Ordered mesoporous silica with robust mechanical and thermal stability, high surface areas, and pore volumes have been successfully used as ordered mesoporous shells for hollow and yolk-shell mesoporous structures. It is well-known that incorporation of aluminum into the silica network can provide ordered mesoporous silica with preferable properties in acidity and stability in various chemical and physical environments.[41−44] Therefore, catalytically active ordered mesoporous aluminosilica shells are a benefit for upgrading and applications of hollow and yolk-shell mesoporous structures. However, hollow and yolk-shell mesoporous structures with ordered mesoporous aluminosilica shells have received only limited success due to the lack of an effective route for controlling morphologies and sizes in mesoporous aluminosilicas.[45] In previous studies, conventional ordered mesoporous aluminosilicas, such as Al-MCM-41, were usually obtained by co-assembly of cationic surfactants, aluminate species, and silicate species in a hot alkaline solution.[43,44] Tetraethyl orthosilicate (TEOS) and sodium silicate (Na_2SiO_3) were the most widely used silica precursors. Although these approaches are easy to control the structure parameters of mesopores, the morphologies of as-synthesized ordered mesoporous aluminosilicas are always irregular. We have recently reported that hollow mesoporous silica spheres can be obtained by alkaline etching solid silica spheres (designated as $sSiO_2$) in the presence of cationic surfactants through co-assembly of cationic surfactants and silicate species produced by etching $sSiO_2$.[33] In this study, we have now revealed that it is also feasible to use premade silica spheres as the silica precursor to fabricate hollow mesoporous aluminosilica spheres.

For the first time, $sSiO_2$ (Figure 1a) obtained by the Stöber method were used as the silica precursor for syntheses of ordered mesoporous aluminosilicas. After going through a facile reaction condition in which $sSiO_2$ were treated with a hot alkaline solution in the presence of $NaAlO_2$ and CTAB, $sSiO_2$ were directly converted into uniform hollow mesoporous aluminosilica spheres/CTAB complexes (designated as [Na]-HMAS/CTAB). This proposed approach is highly reproducible and scalable. Grams of products can be easily prepared in a facile one-pot reaction. The photograph (Figure 1b) shows a dish containing ~2 g of [Na]-HMAS/CTAB. After the hydrothermal treatment and the template removal process, the as-synthesized mesoporous aluminosilica spheres (designated as [Na]-HMAS) possess well-defined spherical shells and

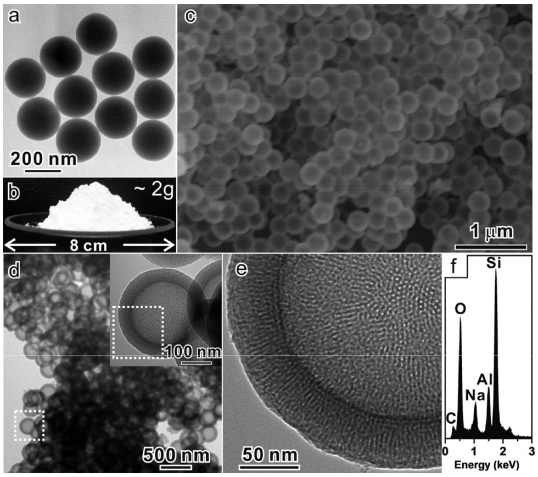

Figure 1. (a) Transmission electron microscopy (TEM) images of *s*SiO$_2$, (b) photo of the as-synthesized [Na]-HMAS/CTAB in a dish, (c) scanning electron microscopy (SEM) image of the as-synthesized [Na]-HMAS (d), and (e) TEM images of the as-synthesized [Na]-HMAS (inset: high-magnification image corresponding to the dashed region), (f) EDX spectrum of the as-obtained [Na]-HMAS.

cavities (Figure 1c,d). The high-magnification TEM image (Figure 1e) reveals that the shells of the [Na]-HMAS display uniform and orderly mesoporous structures. The mesoporous channels in the shell run perpendicular to the surface of [Na]-HMAS. As revealed in the SEM and TEM images, the as-synthesized [Na]-HMAS have a uniform shell with an average thickness of 40 nm. More interestingly, the average inner diameter of the [Na]-HMAS was measured to be 270 ± 10 nm, consistent with the outer diameter of initial *s*SiO$_2$ (Figure S1 in the Supporting Information).

As revealed in the energy-dispersive X-ray spectroscopy (EDX) spectrum (Figure 1f), [Na]-HMAS contains not only Si and Al elements but also Na elements, which agrees well with the conventional sodium form of Al-MCM-41 obtained using sodium-containing precursors [*e.g.*, NaAlO$_2$, sodium hydroxide (NaOH), sodium carbonate (Na$_2$CO$_3$)]. The Al/Si ratio of [Na]-HMAS evaluated from inductively coupled plasma mass spectrometry (ICP) is 0.3, about the maximum Al/Si ratio that can be achieved in [Na]-HMAS. Trying to increase the Al/Si ratio in [Na]-HMAS by supplying more NaAlO$_2$ led to the formation of irregular mesoporous aluminosilica particles as the byproduct of the reaction. It has been reported that the proton form of Al-MCM-41 materials can be obtained by exchanging sodium-containing Al-MCM-41 materials with ammonium cations (NH_4^+) followed by calcination, and the proton form of Al-MCM-41 materials exhibits superior acidity over the sodium form of Al-MCM-41.[43,44] By a similar strategy, we have successfully converted [Na]-HMAS into the proton form of HMAS ([H]-HMAS). TEM analysis (Figure S2) reveals that [H]-HMAS maintained the initial feature of [Na]-HMAS after the ion exchange and calcination processes. As shown by the EDX spectrum

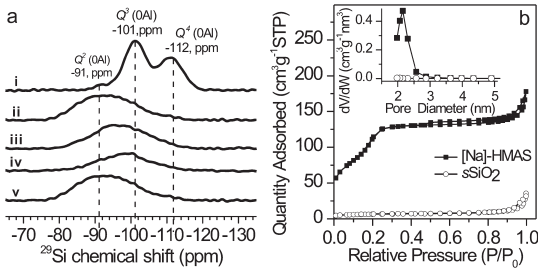

Figure 2. (a) Solid-state 1D ^{29}Si{^{1}H} CPMAS NMR spectra: (i) *s*SiO$_2$, (ii) [Na]-HMAS/CTAB, (iii) [Na]-HMAS/CTAB after the hydrothermal treatment, (iv) [Na]-HMAS, and (v) [H]-HMAS. (b) N$_2$ sorption isotherms of *s*SiO$_2$ and [Na]-HMAS. Inset: pore size distribution.

(Figure S2), [H]-HMAS contains Si and Al elements but no Na elements.

The degree of silica/aluminosilica condensation in the series of HMAS materials was hypothesized to be altered during different post-synthesis treatments, which was monitored by solid-state 1D ^{29}Si{^{1}H} cross-polarization (CP) magic-angle spinning (MAS) nuclear magnetic resonance (NMR) spectroscopy. The ^{29}Si CPMAS NMR spectrum of the *s*SiO$_2$ (Figure 2a(i)) shows three partially resolved ^{29}Si signals centered at −91, −101, and −112 ppm, assigned as Q^2(0Al), Q^3(0Al), and Q^4(0Al) ^{29}Si moieties, respectively. The Q^n(*m*Al) represents a tetrahedral silica unit covalently bonded with *n* next-nearest neighbor Si or Al atoms and *m* next-nearest neighbor Al atoms specifically (an integer value between 0 and *n*) through bridging oxygen atoms.[46,47] The presence of significant ^{29}Si intensity at −101 ppm from Q^3(0Al) ^{29}Si species demonstrates the incomplete cross-linking of silanol species in the silica nanospheres (designated as *s*SiO$_2$). On the other hand, the significantly reduced intensities of Q^3(0Al) and Q^4(0Al) ^{29}Si signals in the ^{29}Si CPMAS NMR spectrum of [Na]-HMAS/CTAB (Figure 2a(ii)) show decreased cross-linking among ^{29}Si species in frameworks and the changes of ^{29}Si environments by Al incorporation, supported by the ICP result (Si/Al = 3.32) and the fact that the ^{29}Si CPMAS NMR spectrum (Figure 2a(ii)) could be contributed from Q^3(0Al), Q^4(1Al), and Q^4(2Al) ^{29}Si species. The cross-linking of the aluminosilica frameworks was further increased after the hydrothermal treatment (designated as [Na]-HMAS/CTAB after the hydrothermal treatment), as established by the broad ^{29}Si signal centered at −97 ppm that appears at slightly lower frequency in the ^{29}Si CPMAS NMR spectrum (Figure 2a(iii)). Similarly, a broad ^{29}Si signal at −99 ppm in the ^{29}Si CPMAS NMR spectrum (Figure 2a(iv)) supports that the degree of aluminosilica condensation was also increased after the subsequent calcination (designated as [Na]-HMAS). In addition, the ^{29}Si{^{1}H} CPMAS NMR spectrum of [Na]-HMAS (Figure 2a(iv)) shows a broad skewed signal at −99 ppm corresponding to a broad distribution of ^{29}Si environments in aluminosilica frameworks. Compared with [Na]-HMAS,

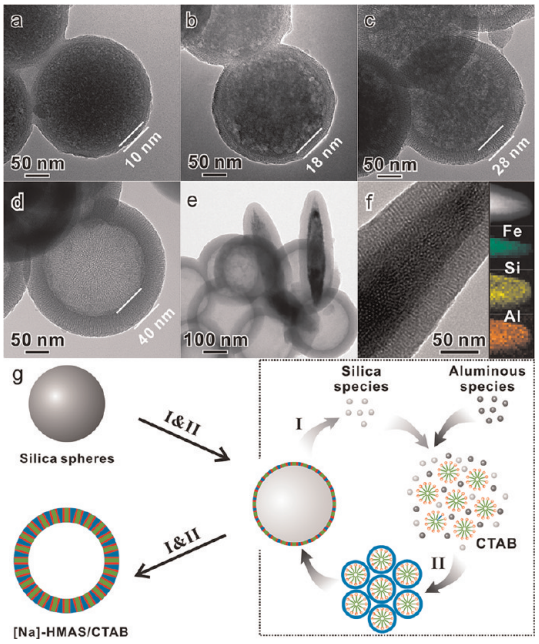

Figure 3. (a–d) TEM images of the morphological evolution in the time-dependent experiments carried out by using 50 mg of $sSiO_2$: (a) 0.5 h, (b) 1 h, (c) 2 h, and (d) 3 h. (e,f) TEM images of the products obtained by the addition of ellipsoid-shaped α-Fe_2O_3 particles. Inset: mapping of elements by EDX analysis under the STEM mode. (g) Schematic illustration for the formation of the HMAS, (I) alkaline etching of silica template, (II) co-assembly of cationic surfactant, aluminate species, and silica species.

the $^{29}Si\{^1H\}$ CPMAS NMR spectrum of [H]-HMAS (Figure 2a(v)) with the increased intensity of the signal at −92 ppm in lower frequencies (*i.e.*, larger parts per million in the ^{29}Si chemical shift) reflects the evidence of reduced cross-linking and increased amounts of protons in the aluminosilica frameworks following the NH_4^+ ion-exchange procedure.

The porosity of [Na]-HMAS was investigated by N_2 adsorption–desorption measurements. [Na]-HMAS exhibits a type IV isotherm with a type H2 hysteresis loop (Figure 2b), characteristic of mesoporous materials. The BET surface areas and pore volumes of [Na]-HMAS are 428.0 $m^2\ g^{-1}$ and 0.34 $cm^3\ g^{-1}$, respectively. The mesoporous feature of [Na]-HMAS is thermally stable at a temperature up to 800 °C. In comparison, the BET surface areas of $sSiO_2$ are only 22.0 $m^2\ g^{-1}$. In addition, [Na]-HMAS has a rather narrow pore size distribution centered at 2.3 nm, as shown by the pore size distribution from the analysis of the adsorption branch of the isotherm using the BJH method. Such a pore size distribution of [Na]-HMAS is similar to conventional Al-MCM-41 materials synthesized using CTAB to direct the formation of mesopores.[43,44] It is noteworthy that, after the ion-exchange and calcination processes, [H]-HMAS still retained the same porosity as [Na]-HMAS, indicating that the ion exchange and calcination treatments did not change the pore structures of HMAS.

Formation Mechanism of HMAS. The formation of HMAS is hypothesized to occur by etching silica cores of $sSiO_2$ under alkaline conditions and meanwhile by co-assembling CTAB, silicate, and aluminate species. To understand such a mechanism, we carried out time-dependent experiments in which samples were collected at different time intervals. After reaction for 0.5 h, $sSiO_2$ were converted into a core–shell structure with an incompact silica sphere covered by a thin layer mesoporous shell (Figure 3a). As reaction time increases, mesoporous shells became thicker, and silica cores were continuously shrunk (Figure 3b–d). The shrinkage of the silica core indicated that $sSiO_2$ were etched gradually under the alkaline reaction condition. We previously reported that the silicate species etch-released from $sSiO_2$ can co-assemble with cationic surfactants in the alkaline solution to form hollow mesoporous silica spheres.[33] It is also believed that the co-assembly of continuously generated silicate species, cationic surfactants, and aluminate species is responsible for the growth of the mesoporous aluminosilica shell on the surface of $sSiO_2$ observed during the formation of HMAS.

To further demonstrate that mesoporous shells were directly produced from such redeposition of silicate species etched from the $sSiO_2$ templates, an elaborate experiment was designed to capture redeposition products by adding ellipsoid-shaped α-Fe_2O_3 into the synthesis procedure. At the end of the reaction, the formation of an ellipsoid-shaped core–shell structure can be clearly observed by TEM (Figure 3e). As revealed by the high-magnification TEM image (Figure 3f), the ellipsoid-shaped α-Fe_2O_3 core was coated by an ordered mesoporous shell. The elemental mapping by EDX analysis confirms the presence of a homogeneous aluminosilica layer on α-Fe_2O_3 particles (inset of Figure 3f). On the basis of the growth process of HMAS, the formation mechanism of HMAS is proposed as illustrated in Figure 3g: (1) The $sSiO_2$ templates were slowly etched under the alkaline condition to provide soluble silicate species. (2) The released soluble silicate species were then co-assembled with cetyltrimethylammonium cations (CTA^+) and aluminate species on the surface of $sSiO_2$ to form thereon the ordered mesoporous aluminosilica shell. (3) As the silica cores of $sSiO_2$ were etched, the ordered mesoporous aluminosilica shell continuously grew until the silica cores of $sSiO_2$ were entirely etched, forming HMAS in the end. On the basis of the proposed formation mechanism, the size of HMAS should be tunable by varying the size of $sSiO_2$ templates. HMAS with hollow interior sizes of 470 and 100 nm were successfully obtained by the same synthesis procedures simply using $sSiO_2$ with particle sizes of 470 and 100 nm as templates, respectively (Figure S3).

Yolk-Shell Structures with Ordered Mesoporous Aluminosilica Shells. Fabricating yolk-shell structures with functional

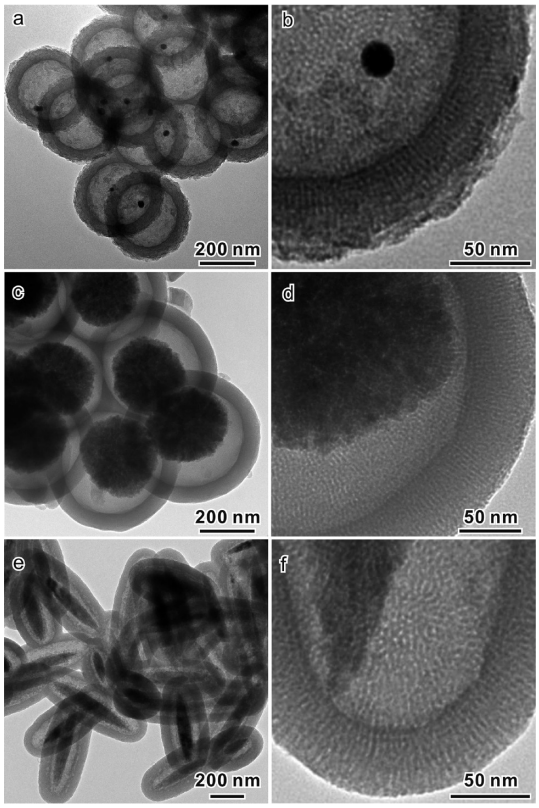

Figure 4. TEM images: (a,b) yolk-shell Au@[Na]-HMAS, (c,d) yolk-shell Fe_3O_4@[Na]-HMAS, and (e,f) yolk-shell α-Fe_2O_3@[Na]-HMAS.

nanoparticles encapsulated in hollow porous shells has been recently demonstrated as an effective method to take advantage of porous materials to broaden applications of nanoparticles.[9−24] Since the simple approach developed in this study allows the direct conversion of *s*SiO_2 into hollow ordered mesoporous structures, functional yolk-shell structures with ordered mesoporous shells can be easily prepared by replacing *s*SiO_2 with silica-coated composites. For instance, when gold-containing silica spheres (designated as Au@SiO_2) were used as templates, well-defined yolk-shell structures with the movable Au yolk nicely encapsulated with aluminosilica shells were obtained (designated as yolk-shell Au@[Na]-HMAS). As revealed by the TEM images (Figure 4a,b and Figure S4), similar to HMAS prepared from *s*SiO_2, aluminosilica shells in obtained yolk-shell structures also consist of ordered pore channels perpendicular to surfaces. It is well-documented that one-in-one encapsulation of noble metal nanoparticles in hollow porous spheres can effectively prevent the aggregation of catalytic particles and therefore significantly improve their catalytic stability.[11−16] Compared with disordered pore channels, perpendicular pore channels in hollow mesoporous shells can shorten diffusion paths of substances and thus fasten their diffusion during catalysis. Accordingly, yolk-shell Au@[Na]-HMAS are expected as promising nanoreactor systems for confined catalysis.

Yolk-shell structures with ordered mesoporous aluminosilica shells can be functionalized for desired applications by encapsulating specific nanoparticles into shells. For example, spherical Fe_3O_4 particles built up from superparamagnetic Fe_3O_4 nanocrystals are a class of desirable magnetic materials for magnetic separation applications.[48,49] Using silica-coated superparamagnetic iron (II, III) oxide (Fe_3O_4) core−shell nanocomposites as the templates, we have successfully obtained yolk-shell structures with superparamagnetic Fe_3O_4 cores inside hollow ordered aluminosilica shells (designated as yolk-shell Fe_3O_4@[Na]-HMAS) shown in Figure 4c,d. The as-synthesized superparamagnetic yolk-shell particles dispersed in solutions can be easily collected by applying an external magnetic field (Figure S5). The combination of magnetic Fe_3O_4 cores and ordered mesoporous aluminosilica shells makes such a material applicable as a magnetically recyclable catalyst and a sorbent. In addition to spherical silica-coated particles, nonspherical silica-coated particles were also applied as the templates for fabricating nonspherical yolk-shell mesoporous structures. As shown in Figure 4e,f, elliptical yolk-shell α-Fe_2O_3 hollow mesoporous aluminosilica particles (designated as α-Fe_2O_3@[Na]-HMAS) were successfully prepared from ellipsoid-shaped α-Fe_2O_3-containing silica core−shell particles.

The synthesis strategy of yolk-shell materials with ordered mesoporous aluminosilica shells functionalized by specific nanoparticles can be applied to not only silica-based but also carbon-based materials. Such carbon-based yolk-shell materials with functional nanoparticles encapsulated in hollow carbon shells have found many applications in catalysis and Li-ion batteries.[16,21] Although mesoporous silica spheres have been successfully used as templates to prepare hollow mesoporous carbon spheres by the incipient wetness impregnation strategy, the chemical decoration of the silica templates with aluminum sites is typically required for carbon deposition.[50,51] The inherent aluminum sites in the ordered mesoporous shells of HMAS make it possible to directly use our aluminosilica-based yolk-shell particles for preparing carbon-based yolk-shell materials. For instance, when yolk-shell Au@[Na]-HMAS was used as the templates and furfuryl alcohol as the carbon precursor, uniform yolk-shell Au-containing carbon particles were successfully obtained by the incipient wetness impregnation strategy (Figure S6). We therefore believe that the synthetic approach reported here is applicable to the syntheses of yolk-shell structures with diverse compositions, morphologies, and functionalities.

Catalytically Active Yolk Protected by Permeable Perpendicular Pore Channels. Yolk-shell structures have been recognized as ideal frameworks to stabilize metal nanoparticle catalysts owing to the structural feature that functional cores are isolated by a permeable

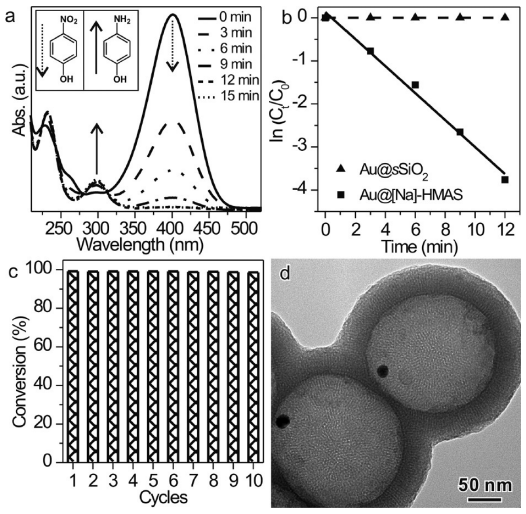

Figure 5. (a) UV−vis spectra showing gradual reduction of 4-nitrophenol with yolk-shell Au@[Na]-HMAS. (b) Plot of $\ln(C_t/C_0)$ *versus* time for yolk-shell Au@[Na]-HMAS and Au@SiO_2. (c) Conversion of 4-nitrophenol in 10 successive cycles of reduction with yolk-shell Au@[Na]-HMAS. (d) TEM image of the finally retrieved yolk-shell Au@[Na]-HMAS.

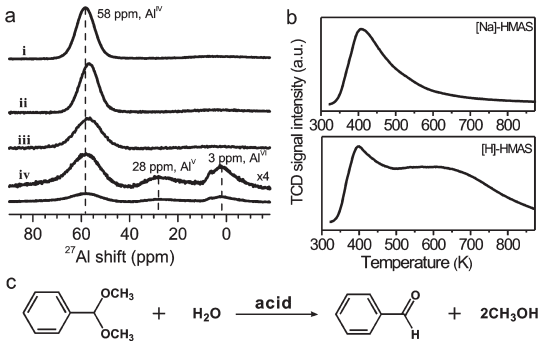

Figure 6. (a) Solid-state 1D single-pulse ^{27}Al MAS NMR spectra: (i) [Na]-HMAS/CTAB, (ii) [Na]-HMAS/CTAB after the hydrothermal treatment, (iii) [Na]-HMAS, (iv) [H]-HMAS. (b) NH_3-TPD of [Na]-HMAS and [H]-HMAS. (c) Scheme of acid-catalyzed deprotection of benzaldehyde dimethyl acetal to benzaldehyde.

porous shell and have relatively homogeneous surrounding environments. Yolk-shell Au@[Na]-HMAS were chosen to demonstrate such stable structures in our yolk-shell materials. The reduction of 4-nitrophenol by sodium borohydride ($NaBH_4$) to 4-aminophenol was chosen as a model reaction to evaluate the catalytic ability and stability of yolk-shell Au@[Na]-HMAS. The reduction process was monitored by UV−vis absorption spectroscopy (Figure 5a). The reduction reaction did not proceed in the absence of Au catalysts, which was evidenced by a constant absorption peak at 400 nm. When yolk-shell Au@[Na]-HMAS were introduced as catalysts into the solution, the intensity of the characteristic absorption peak at 400 nm corresponding to 4-nitrophenol quickly decreased and the characteristic absorption of 4-aminophenol at 295 nm appeared accordingly. The reduction of 4-nitrophenol into 4-aminophenol was completely finished in 12 min, and the color change of bright yellow to colorless was observed. The presence of two isosbestic points at 279 and 313 nm reveals that the reduction proceeded without producing byproducts. A linear relation of $\ln(C_t/C_0)$ *versus* time, where C_t and C_0 are 4-nitrophenol concentrations at time t and 0, respectively, were observed for yolk-shell Au@[Na]-HMAS catalysts (Figure 5b), indicating that the reduction reaction can be considered as a pseudo-first-order reaction,[13] and the rate constant is estimated to be 0.31 min^{-1}. In comparison, as solid silica shells are evidently impermeable to 4-nitrophenol, no measurable catalytic activity of Au@SiO_2 core−shell structures can be detected in the same reduction reaction. These results clearly reveal that ordered mesoporous shells in our yolk-shell Au@[Na]-HMAS are highly permeable to the reaction substances.

In addition to catalytic activity, the structural stability of yolk-shell Au@[Na]-HMAS was also examined. The catalytic recyclability was first investigated by conducting the catalytic reduction of 4-nitrophenol to demonstrate the excellent stability of yolk-shell Au@[Na]-HMAS. As shown in Figure 5c, yolk-shell Au@[Na]-HMAS were still highly active with a conversion over 99% at 12 min even after 10 successive cycles of reactions. The TEM images of the final catalysts reveal that the mesoporous channels and the Au yolk were well retained after 10 repeating catalytic cycles (Figure 5d and Figure S7). More interestingly, we also found that the alkali resistance of ordered mesoporous aluminosilica shells is higher than that of pure silica. The structures of yolk-shell Au@[Na]-HMAS were not destroyed after an alkaline treatment (pH = 12) at 50 °C for 24 h. In contrast, when treating Au@SiO_2 under the same condition, the collapse of silica shells and the aggregation of Au particles were observed (Figure S8). The high catalytic performance and favorable stability of yolk-shell Au@[Na]-HMAS makes the developed synthesis strategy useful for the design of active and stable catalytic nanoreactors.

Acid Activity of Mesoporous Aluminosilica Shells. It is known that ordered mesoporous aluminosilicas have been well-demonstrated as versatile solid acid catalysts owing to their acidity properties.[41−44] In general, the acidity of aluminosilicas depends on the amount of aluminum in frameworks as well as their structures (*e.g.*, four-, five-, or six-coordinate). Here, the acidity properties of HMAS alter with their different preparation conditions, as supported by their varied acid strengths and aluminum structures. ^{27}Al MAS NMR was used to identify coordinations of aluminum in the series of HMAS, and the ^{27}Al MAS NMR spectra show that the only resonance was at ~58 ppm in the as-synthesized [Na]-HMAS/CTAB (Figure 6a(i)), [Na]-HMAS/CTAB after hydrothermal treatment (Figure 6a(ii)), and [Na]-HMAS (Figure 6a(iii)). This indicates that all ^{27}Al species in these types of HMAS are four-coordinate. On the other hand, the [H]-HMAS ([Na]-HMAS after the

NH_4^+ ion-exchange process followed by calcination) have four-, five-, and six-coordinate ^{27}Al species, as evidenced by the three separated ^{27}Al signals at ~58, ~28, and ~3 ppm in the ^{27}Al MAS NMR spectrum, respectively (Figure 6a(iv)). In ordered mesoporous aluminosilicas, four-coordinate ^{27}Al species and five/six-coordinate ^{27}Al species are typically associated with Brønsted and Lewis acid sites, respectively.[43,44] The acid strength of [Na]-HMAS and [H]-HMAS was experimentally investigated by temperature-programmed ammonia desorption (NH_3-TPD). The TPD profile of [Na]-HMAS shows a dominant peak around 400−600 K (Figure 6b), indicating the presence of the Brønsted acid sites in [H]-HMAS.[43,44] The noticeable increase of Brønsted acid sites and the appearance of Lewis acidic sites (peak around 650−750 K)[43,44] observed in the TPD profile of [H]-HMAS (Figure 6b) suggest that both [H]-HMAS and [Na]-HMAS should provide active sites for acid catalysis due to their acidic aluminum sites in the framework, but [H]-HMAS have much more acid sites.

[H]-HMAS are hypothesized to be more acidic than [Na]-HMAS by considering their available protons for donation. To validate the acid catalytic activity of [H]-HMAS and [Na]-HMAS, the acid-catalyzed deprotection of benzaldehyde dimethyl acetal to benzaldehyde was chosen as a probe reaction (Figure 6c). As the acetal is stable in neutral and alkaline conditions, the deprotection reaction does not proceed without acid catalysts.[52] When [Na]-HMAS were used as the acid catalysts, nearly 90% of the benzaldehyde dimethyl acetal was converted into benzaldehyde after a 4 h reaction. In contrast, a full conversion (>99%) of the benzaldehyde dimethyl acetal was achieved within 2 h when the same dosage of [H]-HMAS was used as the catalyst. The higher acid-catalyzed activity of [H]-HMAS can therefore be nicely explained by the superior acidity of [H]-HMAS over [Na]-HMAS. On the basis of these results, [H]-HMAS obtained in this work are promising candidates for solid acid catalysts.

Yolk-Shell Structures for Multistep Reaction Sequences. Mimic natural catalysts (*e.g.*, many enzymes can manipulate a multistep reaction sequence in a single vessel for syntheses of structurally complex organic molecules) have attracted synthetic researchers.[40] Recently, efforts have been made to use base- and acid-functionalized silica as bifunctional catalysts for multistep reaction sequences.[52−55] However, the design of new multifunctional catalysts with either cooperative or independent catalytic performances is still a challenge. In a catalyst for multistep reactions, different reactions are typically catalyzed at different catalytically active sites. With available catalytic activity of the permeable mesoporous aluminosilica shells and adjustable cores, the yolk-shell structures obtained in this work are potential candidates for site separations of multiple catalyst.

Benzimidazole derivatives have attracted increasing interest over recent decades due to their antiviral, antiulcer, and anticancer properties.[56−58] Recently, using recyclable ordered mesoporous aluminosilica (*e.g.*, Al-KIT-5) to replace traditional acid catalysts provides a mild and economical synthesis route to the syntheses of benzimidazole derivatives.[59] To demonstrate that the yolk-shell structures in this work can be used as catalysts for multistep reactions, a synthesis route involving an acid catalysis and catalytic hydrogenation was chosen as a model one-pot reaction sequence for the synthesis of benzimidazole derivatives (Figure 7a). Biologically active compound 2-(4-aminophenyl)-1*H*-benzimidazole, a key intermediate in the syntheses of benzimidazole derivatives,[56−58] was proposed as the target compound.

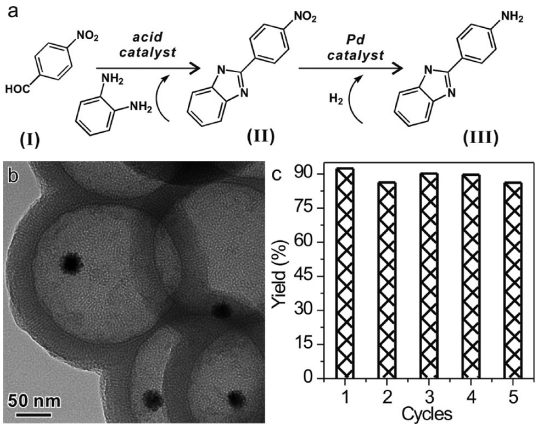

Figure 7. (a) Schematic illustration of the multistep reaction sequence involving an acid catalysis and subsequent catalytic hydrogenation for the synthesis of 2-(4-aminophenyl)-1*H*-benzimidazole. (b) TEM image of Pd/Au@[Na]-HMAS. (c) Synthesis yield of 2-(4-aminophenyl)-1*H*-benzimidazole in the five successive reactions with Pd/Au@[Na]-HMAS.

As the ordered mesoporous aluminosilica shells would serve as acid catalysts, we therefore introduced Pd species for catalytic hydrogenation. In our studies, yolk-shell Au@[Na]-HMAS were chosen as the precursors to simplify Pd incorporation into hollow mesoporous aluminosilica spheres since Au nanoparticles in Au@[Na]-HMAS can serve as the seeds to facilitate the Pd deposition only inside the hollow spheres.[17] Typically, an aliquot of potassium tetrachloropallidate (K_2PdCl_4) was added to an aqueous suspension containing Au@[Na]-HMAS and ascorbic acid under constant stirring at room temperature. During the reaction, the change of the originally reddish suspension into a final dark red one can be directly observed. The TEM images of the isolated final dark red suspension confirmed the confined growth of fine Pd nanoparticles on Au nanoparticles inside the hollow cavity (Figure 7b and Figure S9).

The as-synthesized Pd/Au@[Na]-HMAS were then used as the catalysts for the one-pot two-step synthesis of 2-(4-aminophenyl)-1*H*-benzimidazole from 4-nitrobenzaldehyde and 1,2-phenylenediamine. The intermediate 2-(4-aminophenyl)-1*H*-benzimidazole and the

final product 2-(4-aminophenyl)-1*H*-benzimidazole were identified by mass spectrometry and mass spectrometry and ^{1}H NMR, respectively (Figure S10). After both acid catalysis and hydrogenation steps, nearly 100% conversion of the reactant 4-nitrobenzaldehyde and 92% yield of the desired product 2-(4-aminophenyl)-1*H*-benzimidazole were obtained. In the previous report on the two-step synthesis of 2-(4-aminophenyl)-1*H*-benzimidazole, the total yield was ~80% using nonrecyclable catalysts. Moreover, the relevant synthesis procedure was somewhat time-consuming.[57] In a control experiment, no conversion of reactants was detected in the absence of the catalysts. Although ordered mesoporous aluminosilica shells could catalyze the first step of the two-step reaction sequence, neither [Na]-HMAS nor Au@[Na]-HMAS gave the conversion of the reactants into the final product 2-(4-aminophenyl)-1*H*-benzimidazole. In the absence of Pd components in the catalysts, the intermediate 2-(4-nitrophenyl)-1*H*-benzimidazole was obtained as the main product. When using commercial Pd/C catalyst, the reactants were completely converted into 4-aminobenzaldehyde. These results confirm that the designed localization of Pd functionalities in HMAS indeed leads to an effective catalyst for multistep reaction sequences.

Pd/Au@[Na]-HMAS are hypothesized to have high catalytic activity and chemically stable structures after catalysis cycles as Au@[Na]-HMAS. After the synthesis of 2-(4-aminophenyl)-1*H*-benzimidazole, Pd/Au@[Na]-HMAS were separated by centrifugation, washed with methanol, and redispersed into methanol for the next catalysis cycle. The catalyst Pd/Au@[Na]-HMAS showed high activity in the five successive cycles under the same reaction conditions (Figure 7c). The yield of the products in the fifth cycle was 86%, confirming that the catalytic sites of Pd and mesoporous aluminosilica shell were stable and recyclable.

CONCLUSIONS

In summary, we have developed a facile route to fabricate hollow mesoporous aluminosilica spheres with pore channels perpendicular to surfaces by combining alkaline etching of solid silica spheres and coassembly of cationic surfactants, silicate, and aluminate species on surfaces of solid silica spheres. Such a synthetic strategy is remarkably effective and reproducible, providing a facile route to tailor the size of hollow mesoporous aluminosilica spheres. As-synthesized hollow mesoporous aluminosilica spheres can be used as an acid catalyst, and their acidity can be further improved by the ion-exchange strategy. Furthermore, the proposed strategy can be extended as a general strategy to transform silica-coated nanocomposites into ordered mesoporous yolk-shell structures with diverse functionalities, morphologies, and sizes. The excellent catalytic performance and stability of the reduction of 4-nitrophenol with yolk-shell Au@[Na]-HMAS demonstrate that pore channels perpendicular to surfaces are permeable and yolk-shell structures with ordered mesoporous aluminosilica shells are ideal candidates for nanoreactors. More importantly, on the basis of the available acidity and adjustable yolk, Pd/Au@[Na]-HMAS show high catalytic performances and recyclability in two-step reaction sequences of synthesizing benzimidazole derivatives. The hollow mesoporous aluminosilica structures reported in this work are powerful platforms for nanoreactors, and we believe that the synthesis strategy can be extended to produce new composite materials with enhanced properties for advanced applications.

EXPERIMENTAL METHODS

Chemicals. TEOS, benzaldehyde dimethyl acetal, benzaldehyde, 4-nitrobenzaldehyde, 1,2-phenylenediamine, and benzimidazole were purchased from Alfa Aesar. Ammonia solution (25−28%), CTAB, ethanol, L-ascorbic acid, $NaAlO_2$, Na_2CO_3, and 4-nitrophenol, were purchased from Sinopharm Chemical Reagent Co. (Shanghai, China). All reagents were used without further purification. Deionized water was used in all experiments.

Synthesis of *s*SiO_2. *s*SiO_2 were carried out following a slightly modified Stöber process. In a typical synthesis, 6 mL of TEOS was rapidly added into a mixture of 75 mL of ethanol, 10 mL of deionized water, and 3.15 mL of ammonium aqueous solution and then stirred at room temperature for 1 h, resulting in the formation of a white silica colloidal suspension. The silica particles were centrifugally separated from the suspension and washed with deionized water and ethanol.

Synthesis of [Na]-HMAS/CTAB. The as-synthesized *s*SiO_2 were homogeneously dispersed in deionized water by ultrasonication, followed by the addition of CTAB, and then stirred at room temperature. The mixed solution was homogenized for 30 min to form a uniform dispersion. $NaAlO_2$ and Na_2CO_3 were added to the dispersion with continuous stirring. In the final mixture, the weight ratio of *s*SiO_2/CTAB/$NaAlO_2$/Na_2CO_3/H_2O was 1:0.25:0.53:0.41:200. The mixture was heated at 95 °C with continuous stirring for a certain time, and the products (*i.e.*, [Na]-HMAS/CTAB) were collected by centrifugation. The reaction time was dependent on the dosage of the reactants. For example, when *s*SiO_2 were employed with three different contents of 50 mg/1 g/2.5 g, the corresponding heating times were 3, 16, and 24 h, respectively.

Hydrothermal Treatment for [Na]-HMAS/CTAB. After washing two times with deionized water, 1 g of [Na]-HMAS/CTAB was homogeneously dispersed in 16 mL of deionized water. Then the suspension was transferred into a 20 mL Teflon-lined stainless steel autoclave. After sealing, the autoclave was maintained at 150 °C for 2 days and then cooled to room temperature. The [Na]-HMAS/CTAB were collected by centrifugation and then washed with deionized water and ethanol several times.

CTAB Removal from the Na-HMAS/CTAB. To obtain the pure mesoporous products (*i.e.*, [Na]-HMAS), the as-synthesized [Na]-HMAS/CTAB after the hydrothermal treatment were warmed up at a rate of 1.5 °C min^{-1} and maintained at 550 °C for 6 h in air.

Synthesis of [H]-HMAS. [H]-HMAS were prepared through a two-step method reported previously.[7,8] First, the ammonia form of HMAS was obtained by ion exchanging [Na]-HMAS with NH_4NO_3 aqueous solutions (1 M) at 80 °C for 8 h. The [H]-HMAS were then obtained by deammoniation at 550 °C for 6 h in air.

Synthesis of Ordered Mesoporous Aluminosilicate Yolk-Shell Structures. Yolk-shell Au@[Na]-HMAS, yolk-shell Fe_3O_4@[Na]-HMAS, and yolk-shell Fe_2O_3@[Na]-HMAS were synthesized under similar reaction conditions for HMAS except replacing $sSiO_2$ with Au@SiO_2, Fe_3O_4@SiO_2, and Fe_2O_3@SiO_2. The detailed synthesis procedures of Au@[Na]-HMAS, Fe_3O_4@[Na]-HMAS, Fe_2O_3@[Na]-HMAS, and Au@carbon are provided in the Supporting Information.

Synthesis of Pd/Au@[Na]-HMAS Yolk-Shell Structures. Forty milligrams of Au@[Na]-HMAS and 140 mg of L-ascorbic acid were mixed in 9 mL of deionized water. One milliliter (5 mmol L^{-1}) of K_2PdCl_4 aqueous solution was then added to the mixed suspension and stirred at room temperature for 8 h. The resulting solid Pd/Au@[Na]-HMAS were collected by centrifugation and washed with deionized water and then dried at room temperature under vacuum overnight.

Reduction of 4-Nitrophenol with Yolk-Shell Au@[Na]-HMAS. Ten milligrams of yolk-shell Au@[Na]-HAMS was homogeneously dispersed in 5 mL of deionized water by ultrasonication, followed by the addition of 0.5 mL of $NaBH_4$ aqueous solution (0.5 M), and the mixture was stirred for 10 min at room temperature. Then, 0.25 mL of 4-nitrophenol (0.12 M) was added to the mixture, which was stirred until the deep yellow solution became colorless. During the course of reaction, the reaction progress was monitored by measuring UV–vis absorption spectra of the mixture.

Acid-Catalyzed Deprotection of Benzaldehyde Dimethyl Acetal. Benzaldehyde dimethyl acetal (1 mmol) and water (2.3 mmol) were mixed in 5 mL of toluene at room temperature, followed by the addition of 20 mg of the catalyst ([Na]-HMAS or [H]-HMAS). The resulting mixture was then stirred at reflux temperature for appropriate time. After reaction, the catalyst was separated by centrifugation. The product was analyzed by a GC (FULI 9790II) with capillary column (KB-5, 30 m × 0.32 mm × 0.33 mm).

Synthesis of the 2-(4-Amidophenyl)-1*H*-benzimidazole Using Pd/Au@HMAS Catalyst. Sixty milligrams of Pd/Au@HMAS was dispersed in 5 mL of methanol, followed by the addition of 0.5 mmol of 4-nitrobenzaldehyde and 0.6 mmol of 1,2-phenylenediamine. The resulting mixture was stirred at reflux temperature under air atmosphere for 5 h and then transferred into a glass pressure vessel without any separation or extraction. The vessel was then charged with H_2 to 2 bar reacting for 8 h. After reaction, the reaction mixture was diluted with methanol and the catalyst was separated by centrifugation. The yield of the product was analyzed by HPLC with an internal standard substance (benzimidazole). The product and the internal standard substance were detected by UV spectrum equipped on HPLC. Separation occurred on a Alltima C18 reversed-phase column (150 mm × 4.6 mm internal diameter) using a mobile phase of 35% methanol and 65% distilled water delivered at a rate of 1 mL min^{-1} at 50 °C.

Characterization. SEM and TEM images were taken on a Hitachi S-4800 microscope with a field-emission electron gun and a TECNAI F-30 high-resolution transmission electron microscope operating at 300 kV, respectively. The Al content in the HMAS was quantitatively analyzed by inductively coupled plasma mass spectrometry (ICP). The surface area of the final products was measured by the Brunauer–Emmett–Teller (BET) method using nitrogen adsorption and desorption isotherms on a Micrometrics ASAP 2020 system. Pore size distribution plot was obtained by the Barrett–Joyner–Halenda (BJH) method. The adsorption of ammonia over the products was characterized by temperature-programmed desorption (NH_3-TPD, Micromeritics AUTOCHEM II 2920). The mass spectra were recorded in positive-ion mode on a Bruker-Esquire HCT instrument interfaced by an electrospray ionization source.

Solid-state 1D $^{29}Si\{^1H\}$ CPMAS NMR experiments were conducted on a Bruker AVANCE NMR spectrometer with a 7.0 T wide-bore superconducting magnet, with operating frequencies of 99.38 MHz for ^{29}Si resonances. One-dimensional single-pulse ^{27}Al NMR spectra were collected on a Bruker AVANCE NMR spectrometers with a 18.8 T wide-bore superconducting magnet, with operating at frequencies of 208.53 MHz for ^{27}Al resonances.

Conflict of Interest: The authors declare no competing financial interest.

Acknowledgment. We thank Prof. Bradley F. Chmelka for his help on NMR measurements. We also thank the MOST of China (2011CB932403, 2009CB930703), the NSFC (21131005, 21021061, 20925103), the Fok Ying Tung Education Foundation (121011), the NSF of Fujian Province (Distinguished Young Investigator Grant 2009J06005), and the U.S. National Science Foundation (CHE-0924654) for the financial support.

Supporting Information Available: Synthesis procedures for the $sSiO_2$ with different sizes and yolk-shell Au@[Na]-HMAS, α-Fe_2O_3@[Na]-HMAS, α-Fe_3O_4@[Na]-HMAS, and Au@carbon structures; experimental conditions of solid-state $^{29}Si\{^1H\}$ CPMAS and ^{27}Al NMR measurements; the histogram of size distribution of $sSiO_2$ and [Na]-HMAS; TEM images and EDX of [H]-HMAS; TEM images of [Na]-HMAS obtained by using the $sSiO_2$ with particle sizes of 100 and 470 nm; TEM images of Au@SiO_2 and Au@[Na]-HMAS; photos of Fe_3O_4@[Na]-HMAS enriched by magnet; TEM images of Au@carbon yolk-shell structures; TEM images of Au@[Na]-HMAS suffered 10 successive cycles of reduction of 4-nitrophenol; TEM images of Au@SiO_2 and Au@[Na]-HMAS after treatments with hot alkaline; HRTEM image of Pd/Au@[Na]-HMAS; mass spectrum of 2-(4-nitrophenyl)-1*H*-benzimidazole; mass spectrum and ^1H NMR spectrum of 2-(4-aminophenyl)-1*H*-benzimidazole. This material is available free of charge *via* the Internet at http://pubs.acs.org.

REFERENCES AND NOTES

1. Lou, X. W.; Archer, L. A.; Yang, Z. C. Hollow Micro-/Nanostructures: Synthesis and Applications. *Adv. Mater.* **2008**, *20*, 3987–4019.
2. An, K.; Hyeon, T. Synthesis and Biomedical Applications of Hollow Nanostructures. *Nano Today* **2009**, *4*, 359–373.
3. Kim, S. W.; Kim, M.; Lee, W. Y.; Hyeon, T. Fabrication of Hollow Palladium Spheres and Their Successful Application to the Recyclable Heterogeneous Catalyst for Suzuki Coupling Reactions. *J. Am. Chem. Soc.* **2002**, *124*, 7642–7643.
4. Tang, S. H.; Huang, X. Q.; Chen, X. L.; Zheng, N. F. Hollow Mesoporous Zirconia Nanocapsules for Drug Delivery. *Adv. Funct. Mater.* **2010**, *20*, 2442–2447.
5. Gao, C. B.; Zhang, Q.; Lu, Z. D.; Yin, Y. D. Templated Synthesis of Metal Nanorods in Silica Nanotubes. *J. Am. Chem. Soc.* **2011**, *133*, 19706–19709.
6. Sun, Y. G.; Mayers, B.; Xia, Y. N. Metal Nanostructures with Hollow Interiors. *Adv. Mater.* **2003**, *15*, 641–646.
7. Goldberger, J.; He, R. R.; Zhang, Y. F.; Lee, S. W.; Yan, H. Q.; Choi, H. J.; Yang, P. D. Single-Crystal Gallium Nitride Nanotubes. *Nature* **2003**, *422*, 599–602.
8. Yao, Y.; McDowell, M. T.; Ryu, I.; Wu, H.; Liu, N.; Hu, L. B.; Nix, W. D.; Cui, Y. Interconnected Silicon Hollow Nanospheres for Lithium-Ion Battery Anodes with Long Cycle Life. *Nano Lett.* **2011**, *11*, 2949–2954.
9. Zhao, Y.; Jiang, L. Hollow Micro/Nanomaterials with Multilevel Interior Structures. *Adv. Mater.* **2009**, *21*, 3621–3638.
10. Liu, J.; Qiao, S. Z.; Chen, J. S.; Lou, X. W.; Xing, X.; Lu, G. Q. Yolk/Shell Nanoparticles: New Platforms for Nanoreactors, Drug Delivery and Lithium-Ion Batteries. *Chem. Commun.* **2011**, *47*, 12578–12591.
11. Kamata, K.; Lu, Y.; Xia, Y. N. Synthesis and Characterization of Monodispersed Core–Shell Spherical Colloids with Movable Cores. *J. Am. Chem. Soc.* **2003**, *125*, 2384–2385.
12. Arnal, P. M.; Comotti, M.; Schüth, F. High-Temperature-Stable Catalysts by Hollow Sphere Encapsulation. *Angew. Chem., Int. Ed.* **2006**, *45*, 8224–8227.
13. Lee, J.; Park, J. C.; Song, H. A Nanoreactor Framework of a Au@SiO_2 Yolk/Shell Structure for Catalytic Reduction of *p*-Nitrophenol. *Adv. Mater.* **2008**, *20*, 1523–1528.
14. Huang, X. Q.; Guo, C. Y.; Zuo, J. Q.; Zheng, N. F.; Stucky, G. D. An Assembly Route to Inorganic Catalytic Nanoreactors Containing Sub-10-nm Gold Nanoparticles with Anti-aggregation Properties. *Small* **2009**, *5*, 361–365.
15. Park, J. C.; Song, H. Metal@Silica Yolk–Shell Nanostructures as Versatile Bifunctional Nanocatalysts. *Nano Res.* **2011**, *4*, 33–49.

16. Ikeda, S.; Ishino, S.; Harada, T.; Okamoto, N.; Sakata, T.; Mori, H. K. S.; Torimoto, T.; Matsumura, M. Ligand-Free Platinum Nanoparticles Encapsulated in a Hollow Porous Carbon Shell as a Highly Active Heterogeneous Hydrogenation Catalyst. *Angew. Chem., Int. Ed.* **2006**, *45*, 7063–7066.
17. Yeo, K. M.; Choi, S.; Anisur, R. M.; Kim, J.; Lee, I. S. Surfactant-Free Platinum-on-Gold Nanodendrites with Enhanced Catalytic Performance for Oxygen Reduction. *Angew. Chem., Int. Ed.* **2011**, *50*, 745–748.
18. Lou, X. W.; Yuan, C.; Archer, L. A. Double-Walled SnO_2 Nano-Cocoons with Movable Magnetic Cores. *Adv. Mater.* **2007**, *19*, 3328–3332.
19. Liu, J.; Qiao, S. Z.; Hartono, S. B.; Lu, G. Q. Monodisperse Yolk−Shell Nanoparticles with a Hierarchical Porous Structure for Delivery Vehicles and Nanoreactors. *Angew. Chem., Int. Ed.* **2010**, *49*, 4981–4985.
20. Li, W.; Deng, Y.; Wu, Z.; Qian, X.; Yang, J.; Wang, Y.; Gu, D.; Zhang, F.; Tu, B.; Zhao, D. Hydrothermal Etching Assisted Crystallization: A Facile Route to Functional Yolk-Shell Titanate Microspheres with Ultrathin Nanosheets-Assembled Double Shells. *J. Am. Chem. Soc.* **2011**, *133*, 15830–15833.
21. Zhang, W. M.; Hu, J. S.; Guo, Y. G.; Zheng, S. F.; Zhong, L. S.; Song, W. G.; Wan, L. Tin-Nanoparticles Encapsulated in Elastic Hollow Carbon Spheres for High-Performance Anode Material in Lithium-Ion Batteries. *Adv. Mater.* **2008**, *20*, 1160–1165.
22. Kim, J.; Piao, Y.; Lee, N.; Park, Y. I.; Lee, I. H.; Lee, J. H.; Paik, S. R.; Hyeon, T. Magnetic Nanocomposite Spheres Decorated with NiO Nanoparticles for a Magnetically Recyclable Protein Separation System. *Adv. Mater.* **2010**, *22*, 57–60.
23. Zhu, Y. F.; Ikoma, T.; Hanagata, N.; Kaskel, S. Rattle-Type Fe_3O_4@SiO_2 Hollow Mesoporous Spheres as Carriers for Drug Delivery. *Small* **2010**, *6*, 471–478.
24. Tan, L. F.; Chen, D.; Liu, H. Y.; Tang, F. Q. A Silica Nanorattle with a Mesoporous Shell: An Ideal Nanoreactor for the Preparation of Tunable Gold Cores. *Adv. Mater.* **2010**, *22*, 4885–4889.
25. Liu, J.; Yang, H. Q.; Kleitz, F.; Chen, Z. G.; Yang, T. Y.; Strounina, E.; Lu, G. Q.; Qiao, S. Z. Yolk-Shell Hybrid Materials with a Periodic Mesoporous Organosilica Shell: Ideal Nanoreactors for Selective Alcohol Oxidation. *Adv. Funct. Mater.* **2012**, *22*, 591–599.
26. Wu, X. J.; Xu, D. S. Soft Template Synthesis of Yolk/Silica Shell Particles. *Adv. Mater.* **2010**, *22*, 1516–1520.
27. Qiao, S. Z.; Lin, C. X.; Jin, Y. G.; Li, Z.; Yan, Z. M.; Hao, Z. P.; Huang, Y. N.; Lu, G. Q. Surface-Functionalized Periodic Mesoporous Organosilica Hollow Spheres. *J. Phys. Chem. C* **2009**, *113*, 8673–8682.
28. Yin, Y. D.; Rioux, R. M.; Erdonmez, C. K.; Hughes, S.; Somorjai, G. A.; Alivisatos, A. P. Formation of Hollow Nanocrystals through the Nanoscale Kirkendall Effect. *Science* **2004**, *304*, 711–714.
29. Li, J.; Zeng, H. C. Hollowing Sn-Doped TiO_2 Nanospheres *via* Ostwald Ripening. *J. Am. Chem. Soc.* **2007**, *129*, 15839–15847.
30. Ding, S. J.; Chen, J. S.; Qi, G. G.; Duan, X. N.; Wang, Z. Y.; Giannelis, E. P.; Archer, L. A.; Lou, X. W. Formation of SnO_2 Hollow Nanospheres Inside Mesoporous Silica Nanoreactors. *J. Am. Chem. Soc.* **2010**, *133*, 21–23.
31. Zhang, Q.; Lee, I.; Ge, J. P.; Zaera, F.; Yin, Y. D. Surface-Protected Etching of Mesoporous Oxide Shells for the Stabilization of Metal Nanocatalysts. *Adv. Funct. Mater.* **2010**, *20*, 2201–2214.
32. Chen, Y.; Chen, H. R.; Guo, L. M.; He, Q. J.; Chen, F.; Zhou, J.; Feng, J. W.; Shi, J. L. Hollow/Rattle-Type Mesoporous Nanostructures by a Structural Difference-Based Selective Etching Strategy. *ACS Nano* **2010**, *4*, 529–539.
33. Fang, X. L.; Chen, C.; Liu, Z. H.; Liu, P. X.; Zheng, N. F. A Cationic Surfactant Assisted Selective Etching Strategy to Hollow Mesoporous Silica Spheres. *Nanoscale* **2011**, *3*, 1632–1639.
34. Wong, Y. J.; Zhu, L. F.; Teo, W. S.; Tan, Y. W.; Yang, Y. H.; Wang, C.; Chen, H. Y. Revisiting the Stöber Method: Inhomogeneity in Silica Shells. *J. Am. Chem. Soc.* **2011**, *133*, 11422–11425.
35. Caruso, F.; Caruso, R. A.; Möhwald, H. Nanoengineering of Inorganic and Hybrid Hollow Spheres by Colloidal Templating. *Science* **1998**, *282*, 1111–1114.
36. Taguchi, A.; Schüth, F. Ordered Mesoporous Materials in Catalysis. *Microporous Mesoporous Mater.* **2005**, *77*, 1–45.
37. Liu, R.; Zhao, X.; Wu, T.; Feng, P. Y. Tunable Redox-Responsive Hybrid Nanogated Ensembles. *J. Am. Chem. Soc.* **2008**, *130*, 14418–14419.
38. Liu, R.; Zhang, Y.; Zhao, X.; Agarwal, A.; Mueller, L. J.; Feng, P. Y. pH-Responsive Nanogated Ensemble Based on Gold-Capped Mesoporous Silica through an Acid-Labile Acetal Linker. *J. Am. Chem. Soc.* **2010**, *132*, 1500–1501.
39. Yamada, Y.; Mizutani, M.; Nakamura, T.; Yano, K. Mesoporous Microcapsules with Decorated Inner Surface: Fabrication and Photocatalytic Activity. *Chem. Mater.* **2010**, *22*, 1695–1703.
40. Voit, B. Sequential One-Pot Reactions Using the Concept of "Site Isolation". *Angew. Chem., Int. Ed.* **2006**, *45*, 4238–4240.
41. Zhang, Z.; Han, Y.; Xiao, F. S.; Qiu, S.; Zhu, L.; Wang, R.; Yu, Y.; Zhang, Z.; Zou, B.; Wang, Y.; Sun, H.; Zhao, D.; Wei, Y. Mesoporous Aluminosilicates with Ordered Hexagonal Structure, Strong Acidity, and Extraordinary Hydrothermal Stability at High Temperatures. *J. Am. Chem. Soc.* **2001**, *123*, 5014–5021.
42. Srinivasu, P.; Alam, S.; Balasubramanian, V. V.; Velmathi, S.; Sawant, D. P.; Böhlmann, W.; Mirajkar, S. P.; Ariga, K.; Halligudi, S. B.; Vinu, A. Novel Three Dimensional Cubic *Fm*3*m* Mesoporous Aluminosilicates with Tailored Cage Type Pore Structure and High Aluminum Content. *Adv. Funct. Mater.* **2008**, *18*, 640–651.
43. Sakthivel, A.; Dapurkar, S. E.; Gupta, N. M.; Kulshreshtha, S. K.; Selvam, P. The Influence of Aluminium Sources on the Acidic Behaviour as Well as on the Catalytic Activity of Mesoporous H-AlMCM-41 Molecular Sieves. *Microporous Mesoporous Mater.* **2003**, *65*, 177–187.
44. Wang, Y. R.; Lang, N.; Tuel, A. Nature and Acidity of Aluminum Species in AlMCM-41 with a High Aluminum Content (Si/Al = 1.25). *Microporous Mesoporous Mater.* **2006**, *93*, 46–54.
45. Li, Y.; Shi, J.; Hua, Z.; Chen, H.; Ruan, M.; Yan, D. Hollow Spheres of Mesoporous Aluminosilicate with a Three-Dimensional Pore Network and Extraordinarily High Hydrothermal Stability. *Nano Lett.* **2003**, *3*, 609–612.
46. Engelhardt, G.; Michel, D. *High-Resolution Solid-State NMR of Silicates and Zeolites*; Wiley: Chichester, UK, 1987.
47. Janicke, M. T.; Landry, C. C.; Christiansen, S. C.; Kumar, D.; Stucky, G. D.; Chmelka, B. F. Aluminum Incorporation and Interfacial Structures in MCM-41 Mesoporous Molecular Sieves. *J. Am. Chem. Soc.* **1998**, *120*, 6940–6951.
48. Deng, Y. H.; Qi, D. W.; Deng, C. H.; Zhang, X. M.; Zhao, D. Y. Superparamagnetic High-Magnetization Microspheres with an Fe_3O_4@SiO_2 Core and Perpendicularly Aligned Mesoporous SiO_2 Shell for Removal of Microcystins. *J. Am. Chem. Soc.* **2008**, *130*, 28–29.
49. Fang, W. J.; Chen, X. L.; Zheng, N. F. Superparamagnetic Core−Shell Polymer Particles for Efficient Purification of His-Tagged Proteins. *J. Mater. Chem.* **2010**, *20*, 8624–8630.
50. Yoon, S. B.; Sohn, K.; Kim, J. Y.; Shin, C.-H.; Yu, J.-S.; Hyeon, T. Fabrication of Carbon Capsules with Hollow Macroporous Core/Mesoporous Shell Structures. *Adv. Mater.* **2002**, *14*, 19–21.
51. Guo, L. M.; Zhang, L. X.; Zhang, J. M.; Zhou, J.; He, Q. J.; Zeng, S. Z.; Cui, X. Z.; Shi, J. L. Hollow Mesoporous Carbon Spheres: An Excellent Bilirubin Adsorbent. *Chem. Commun.* **2009**, *40*, 6071–6073.
52. Huang, Y. L.; Xu, S.; Lin, V. S. Y. Bifunctionalized Mesoporous Materials with Site-Separated Brønsted Acids and Bases: Catalyst for a Two-Step Reaction Sequence. *Angew. Chem., Int. Ed.* **2011**, *50*, 661–664.
53. Zeidan, R. K.; Hwang, S. J.; Davis, M. E. Multifunctional Heterogeneous Catalysts: SBA-15-Containing Primary Amines and Sulfonic Acids. *Angew. Chem., Int. Ed.* **2006**, *45*, 6332–6335.

54. Shylesh, S.; Wagener, A.; Seifert, A.; Ernst, S.; Thiel, W. R. Mesoporous Organosilicas with Acidic Frameworks and Basic Sites in the Pores: An Approach to Cooperative Catalytic Reactions. *Angew. Chem., Int. Ed.* **2010**, *49*, 184–187.
55. Shiju, N. R.; Alberts, A. H.; Khalid, S.; Brown, D. R.; Rothenberg, G. Mesoporous Silica with Site-Isolated Amine and Phosphotungstic Acid Groups: A Solid Catalyst with Tunable Antagonistic Functions for One-Pot Tandem Reactions. *Angew. Chem., Int. Ed.* **2011**, *50*, 9615–9619.
56. Pan, W. T.; Miao, H. Q.; Xu, Y. J.; Navarro, E. C.; Tonra, J. R.; Corcoran, E.; Lahiji, A.; Kussie, P.; Kiselyov, A. S.; Wong, W. C.; Liu, H. 1-[4-(1*H*-Benzoimidazol-2-yl)-phenyl]-3-[4-(1*H*-benzoimidazol-2-yl)-phenyl]-urea Derivatives as Small Molecule Heparanase Inhibitors. *Bioorg. Med. Chem. Lett.* **2006**, *16*, 409–412.
57. Bellina, F.; Calandri, C.; Cauteruccio, S.; Rossi, R. Efficient and Highly Regioselective Direct C-2 Arylation of Azoles, Including Free (NH)-Imidazole, -Benzimidazole and -Indole, with Aryl Halides. *Tetrahedron* **2007**, *63*, 1970–1980.
58. Ayhan-Klcgil, G.; Altanlar, N. Synthesis and Antimicrobial Activities of Some New Benzimidazole Derivatives. *Il Farmaco* **2003**, *58*, 1345–1350.
59. Chari, M. A.; Shobha, D.; Kenawy, E. R.; Al-Deyab, S. S.; Reddy, B. V. S.; Vinu, A. Nanoporous Aluminosilicate Catalyst with 3D Cage-Type Porous Structure as an Efficient Catalyst for the Synthesis of Benzimidazole Derivatives. *Tetrahedron Lett.* **2010**, *51*, 5195–5199.